Role of quantum fluctuations in the vortex solid to vortex liquid transition of type-II superconductors

B. J. Taylor, D. J. Scanderbeg, and M. B. Maple
Department of Physics and Institute for Pure and Applied Physical Sciences, University of California, San Diego, La Jolla, California 92093, USA

C. Kwon
Department of Physics and Astronomy, California State University, Long Beach, California 90840, USA

Q. X. Jia
Superconductivity Technology Center, Los Alamos National Laboratory, Los Alamos, New Mexico 87545, USA
(Received 27 July 2006; published 24 July 2007)

The evolution of vortex dynamic properties along the vortex-glass melting lines, $H_g(T)$, of epitaxial thin film $Y_{1-x}Pr_xBa_2Cu_3O_{6.97}$ samples ($x=0-0.4$) and that of an ultrahigh purity oxygen deficient $YBa_2Cu_3O_{6.5}$ single crystal are examined in magnetic fields up to 45 T. Analysis was carried out in the context of a modified melting line expression based on the quantum-thermal-fluctuation model of Blatter and Ivlev [Phys. Rev. B **50**, 10272 (1994)]. The melting line equation developed here provides a means of experimentally determining the physical mechanism responsible for the energy scale which limits vortex motion at high frequencies. It is found that the effective vortex mass is enhanced significantly by quantum fluctuations and that the distance over which quantum fluctuations displace a segment of the vortex flux line is of the order of the size of the vortex core, which *increases* as $T \rightarrow T_c$. Supportive evidence that the equation developed here provides a universal description of the melting line in type-II superconductors is found by analyzing vortex-glass melting line data from a MgB_2 bulk sample and an amorphous α-Mo_xSi_{1-x} film.

DOI: 10.1103/PhysRevB.76.014518 PACS number(s): 74.25.Qt, 74.72.−h

I. INTRODUCTION

After nearly two decades since the discovery of high temperature superconductivity, the phase diagram of vortex matter in type-II superconductors continues to be a source of debate. Certainly, the most experimentally and theoretically investigated feature of the phase diagram is the vortex lattice (or vortex glass) melting line, $H_m(T)$ [$H_g(T)$], the boundary at which the vortex matter undergoes a change from an immobile solid state to an electrically dissipative liquid state. Achieving an understanding of the nature of this transition over the entire range of magnetic field and temperature, within materials with disparate normal state and superconducting properties, and with various types of disorder is of the utmost importance if a truly universal picture of the vortex matter phase diagram is to be developed.

It is well understood that disorder within the superconductor is an important aspect of the physical picture under consideration. In a sufficiently clean superconductor, vortex lines will penetrate the sample in a regular array forming a lattice. As the temperature of the sample is increased, eventually the vortex lattice will undergo a first order melting transition, with a corresponding jump in entropy and magnetization.[1,2] The introduction of disorder or defects into a superconducting sample creates regions to which the normal cores of the vortices are attracted, pinning the vortex to the site and producing a barrier to motion; this enhances the ability of the sample to carry an electrical current without dissipation, and subsequently, destroys the long-range order of the vortex lattice. The result is a variety of glassy vortex states.[3] The glassy phases can each be characterized by an exponent μ, describing their dynamical response where, as an applied current density goes to zero, the defect barriers impeding vortex motion diverge, $U(j \rightarrow 0) \sim U_c(j_c/j)^{\mu}$, and the vortex velocity goes to zero as $v \propto \exp[-U(j)/T]$. Alternatively, the effect of defect barriers on the dynamical properties of the vortices can be described via a critical exponent $\tilde{s}$ characterizing the vanishing of resistivity as the temperature approaches from above a critical value, T_g, so that $\rho(T) \sim (T-T_g)^{\tilde{s}}$. The critical exponent $\tilde{s}$ is itself a product of the static critical exponent ν and, depending on the kind of vortex glass, a factor composed of an expression involving the dynamical exponent z, the dimensionality of the system d, and an anisotropy exponent ζ.

The introduction of random point disorder results in the "original" vortex glass (VG) considered by Fisher *et al.*[4,5] Correlated columnar disorder, such as that introduced by ion bombardment, produces the Bose-glass (BG) state.[6] In the case of extremely weak point disorder, the vortex lattice, while distorted, is able to maintain short range order and is characterized by the absence of lattice dislocations. The preservation of long-range periodicity is sufficient so that Bragg diffraction peaks are observed in scattering experiments, hence, the name Bragg glass.[7] The pinning environments within a vortex glass and a Bose glass differ significantly in that point disorder encourages wandering of the vortex through the sample to seek out pinning centers, but, in contrast, columnar defects inhibit line wandering. Additionally, point disorder is isotropic with respect to the direction of the vortex lines, but columnar disorder produces an anisotropic environment within a few degrees of the alignment of the field to the columns, with corresponding angular dependences.

In spite of the difference of dynamical properties within the region of the melting transitions, the vortex glass and Bose glass are described by a critical behavior with a very similar formalism, based on the critical scaling properties of the superfluid density, resulting only in differing expressions for the critical exponents.[5,6,8] It has been shown that the vortex-glass phase is recovered from the Bose-glass phase as correlated disorder becomes irrelevant, either by strong point disorder or the absence of correlated disorder.[9] The theoretical foundation employed to describe the Bragg-glass state arises from the weak disorder case of the same Hamiltonian that was originally proposed to describe the vortex-glass state.[7,10] While the Bragg glass is expected to undergo a first order melting transition to a vortex liquid with increasing temperature, some experimental evidence and theoretical models suggest that the vortex-glass state lies in a narrow region between the Bragg-glass region and the melting line.[11,12] Even though these three solid vortex phases have distinct properties, it should be apparent that the dynamical properties of the vortices in the melting region of each kind of glass are quite related. Henceforth, we shall use the term vortex glass to encompass both the vortex- and Bose-glass ensembles, keeping in mind the different critical exponents, and shall leave the Bragg glass as a separate case for now. We shall use VG or BG to indicate a specific type of vortex glass.

Theoretical analysis of the problem of the melting transition is complicated, and a consistent theory describing a melting scenario is known for only a few special cases, the pancake-vortex system, treated via a self-consistent stability analysis,[13] and a dislocation-mediated melting scenario in two dimensions[14] and in three dimensions.[15] The latter case allows for a unified phase diagram that includes all three vortex phases. However, this theory does not provide an explicit temperature dependent form of the vortex glass to vortex liquid transition.

In the absence of a consistent theory, a Lindemann-type criterion is often employed. This criterion predicts a melting transition generally when the mean squared amplitude of fluctuations of a lattice approaches a sizable fraction of the lattice constant a_0, $\langle u^2(T_m)\rangle \approx c_L^2 a_0^2$, where $c_L \sim 0.1-0.3$ [$a_0 \approx (\Phi_0/B)^{1/2}$ for a vortex lattice]. A Lindemann-type analysis of vortex flux line displacements leads to the classical thermal fluctuation result,[16,17]

$$B_m \approx \beta_m (c_L^4/G_i) H_{c2}(0)(1-t)^2,$$

where $G_i = [T_c/H_c^2(0)\epsilon\xi^3(0)]^2/2$ is the Ginzburg number, $\xi(0)$ is the in-plane superconducting coherence length, $H_c(0)$ and $H_{c2}(0)$ are the thermodynamic and upper critical fields, and $\beta_m \approx 2.5$.[18]

The Lindemann criterion approach has resulted in many theoretically and phenomenologically derived expressions that are expected to describe the shape of the vortex lattice melting line, $H_g(T)$, over specific ranges of magnetic field and temperature and for various specific material conditions. For example, by taking into account the dominant conditions for each of the three cases of an electromagnetically coupled layered superconductor, a Josephson coupled layered superconductor, and a continuous anisotropic superconductor, three separate expressions are found to describe each scenario.[10] The first two cases describe the mid-temperature/field and high-temperature/low-field regions of a weakly coupled superconductor, respectively. The latter case describes the mid- to high-temperature/mid- to low-field region of a well coupled (anisotropic) superconductor. Each of the two cases then gives way to a two-dimensional expression for the melting line at low temperatures/high fields.

More recent (Lindemann criterion based) theoretical efforts have arrived at quite different expressions for the vortex lattice and/or glass melting line, each of which also breaks the melting line into two or three segments, to account for dominant behavior in the various field and/or temperature regions.[19,20] In addition to accounting for the effects of disorder on destroying the vortex solid phase, the only source of vortex displacements considered in these models are thermal fluctuations.

Blatter and Ivlev showed some time ago that quantum fluctuations are also a relevant source of vortex-line displacements, particularly in the high-T_c superconductors.[18,21] It should be understood that the vortex lattice melting line proposed by Blatter and Ivlev is not an interpolation formula between quantum and classical limits. Instead, quantum fluctuations are accounted for by going to a dynamical description where the relevant functional is the Euclidean action. The quantum problem is then a $(d+1)$-dimensional generalization of the d-dimensional classical problem with the additional dimension describing the dynamics of the system (in imaginary time). The model proposed by Blatter and Ivlev shows that quantum fluctuations are present for all temperatures, but are most relevant above a characteristic magnetic field. In the high-T_c cuprates, they find that this field is $\sim 2-3$ T, so quantum fluctuations must be accounted for over the majority of the melting line.

In a recent paper,[22] we presented experimental data of the vortex-glass melting lines, $H_g(T)$, of the high-T_c $Y_{1-x}Pr_xBa_2Cu_3O_{6.97}$ $(0 \leqslant x \leqslant 0.4)$ and $YBa_2Cu_3O_{6.5}$ systems in magnetic fields up to 45 T, corresponding to a temperature range as large as $0.03 < T/T_c < 1$, and demonstrated that the *entire* $H_g(T)$ line of all samples could be described by a modified form of the vortex lattice melting line expression arrived at by Blatter and Ivlev in their initial work.[21] (It should be noted that they arrived at a second similar expression for the vortex lattice melting line in later work, which is due to a more thorough treatment of the problem.[18]) The key modification involves the introduction of a single vortex-line relaxation time (SVRT) of the form

$$\tau_r^v = \tau_0 \left(\frac{T}{T_c}\right)^s \left(1 - \frac{T}{T_c}\right)^{-s}, \quad (1)$$

which is evaluated along the melting line at $T = T_g$. We then briefly developed an expression for the vortex lattice melting line based on the idea that the underlying physics of the vortex lattice melting line transition involves both the quantum and thermal nature of vortex-line displacements, as described by Blatter and Ivlev,[18,21] and the fluctuation conductivity associated with the zero field superconducting

transition as the critical temperature T_c is approached. An argument is made where the critical behavior of the fluctuation conductivity is responsible for the relaxation time properties of the single vortex lines in the melting region, and this leads to an expression for the relaxation time τ_r^v that is in agreement with that found experimentally [Eq. (1)]. The explanation of the observed behavior of the vortex-line relaxation time in terms of the critical fluctuation conductivity then provides a natural relation between the exponent s and the critical exponent of the VG or BG models, which characterizes the vanishing of resistivity $\rho \sim (T-T_g)^{s_{VG,BG}}$ at the critical temperature T_g. The resulting expression describes the vortex-glass melting lines by three characteristic fitting parameters: the quantum parameter $Q \propto Q_u/\sqrt{G_i}$, a critical exponent s, and the Lindemann number c_L. Generically, it can be seen that a change in dimensionality of the vortex fluctuations along the melting line must be accompanied by a corresponding change in the critical exponent $s_{VG,BG}$.

In this paper, starting from the latter work of Blatter and Ivlev,[18] we develop the melting line equation[22] in greater detail and examine the information it reveals about vortex matter in the $Y_{1-x}Pr_xBa_2Cu_3O_{6.97}$ and $YBa_2Cu_3O_{6.5}$ systems. Additionally, we demonstrate further evidence that the equation provides a universal description of the melting line in type-II superconductors by fitting to melting line data from a diverse collection of systems. The model we develop here is expected to encompass all three vortex-glass phases: the point disorder dominated vortex glass, the correlated disorder dominated Bose glass, and the well ordered Bragg glass.

II. EXPERIMENTAL DETAILS

Epitaxial thin film $Y_{1-x}Pr_xBa_2Cu_3O_{6.97}$ samples ($x=0-0.4$) grown on $LaAlO_3$ substrates by pulsed laser ablation, as well as an ultrahigh purity oxygen deficient $YBa_2Cu_3O_{6.5}$ single crystal grown in a $BaZrO_3$ crucible, were investigated in magnetic fields up to 45 T. The $H_g(T)$ line was established from electrical transport measurements with $H \| c$. For magnetic fields $H \leqslant 9$ T, resistivity $\rho(H,T)$ data were taken in our laboratory at UCSD with fixed field H, and temperature in steps. High-field $\rho(H,T)$ data were taken at the National High Magnetic Field Laboratory (Tallahassee, FL) in a 30 T resistive magnet and a 45 T hybrid magnet. In these systems, the temperature was held fixed and the field was swept at 3 T/min while continuously measuring $\rho(H)$. The values of (T_g,H_g) were determined in low fields by the scaling relation $\rho(T) \sim (T-T_g)^s$ $[s \equiv \nu(z+2-d)]$ of Fisher-Fisher-Huse (FFH).[5] For the high-field data, in which the field was swept, these values were obtained both by a similar expression $\rho(H) \sim (H-H_g)^s$ and directly from the data where $\rho(H) \to 0$. The films were etched lithographically to form resistance bridges with six terminals with sample dimensions $\ell \times w \times t = 0.50 \times 0.010 \times [(1.2-2) \times 10^{-5}]$ cm^3. The $YBa_2Cu_3O_{6.5}$ single crystal dimensions are $0.21 \times 0.076 \times (7.6 \times 10^{-4})$ cm^3. The current values used were $I=10$ μA and 10 mA, respectively, corresponding to current densities of $J \lesssim 90$ A/cm^2 and $J \approx 2$ A/cm^2. The current density and electric field values used here were well below the criteria of $J_d \sim 10^5$ A/cm^2 and $E \sim 10^{-1}$ V/cm for films and $J_d \sim 10^2$ A/cm^2 and $E \sim 10^{-6}$ V/cm established by Charalambous *et al.*[23]

III. MODEL

We begin by briefly restating the vortex lattice melting problem as approached by Blatter and Ivlev.[18,21] In order to account for the contribution of quantum fluctuations to the mean squared displacement $\langle u^2 \rangle$ of the single vortex line beyond the standard path integral formulation, a dynamical description is needed. The relevant functional is the Euclidean action $\mathcal{S}[\mathbf{u}]$, in Matsubara representation,

$$\frac{\mathcal{S}[\mathbf{u}]}{\hbar} = \frac{1}{T}\sum_n \{\mathcal{T}[\mathbf{u_n}] + \mathcal{F}[\mathbf{u_n}]\}, \tag{2}$$

with the dynamical term $\mathcal{T}[\mathbf{u_n}]$ given by

$$\mathcal{T}[\mathbf{u_n}] = \frac{1}{2}\int \frac{d^3k}{(2\pi)^3}\{[\mu(\omega_n)\omega_n^2 + \eta(\omega_n)|\omega_n|]|\mathbf{u_n}(\mathbf{k})|^2\}$$

and the elastic free energy of the system, $\mathcal{F}[\mathbf{u}]$, given by

$$\mathcal{F}[\mathbf{u}] = \frac{1}{2}\int \frac{d^3k}{(2\pi)^3}\{c_{11}(\mathbf{k})[\mathbf{K}\cdot\mathbf{u}]^2 + c_{66}(\mathbf{k})[\mathbf{K}_\perp\cdot\mathbf{u}]^2 + c_{44}(\mathbf{k})[k_z\cdot\mathbf{u}]^2\},$$

with c_{66} denoting the shear moduli, $c_{11}(\mathbf{k})$ and $c_{44}(\mathbf{k})$ the dispersive compression and tilt moduli, respectively, $\mathbf{u}(\mathbf{k})$ the Fourier transform of the classical displacement field $\mathbf{u}(\mathbf{r})$, $\mathbf{k}=(\mathbf{K},k_z)$, and $\mathbf{K}_\perp=(k_y,-k_x)$.

The summation over Matsubara frequencies will be cut off by either the kinetic mass term $\mu(\omega_n)\omega_n^2$ or the intrinsic cutoff arising from the gap energy Δ, where Ω is given by $\Omega=\min[\Omega_\mu,\Omega_\Delta]$. The kinetic cutoff frequency is given by $\Omega_\mu \approx \sqrt{\eta_\ell/\mu_\ell\tau_r}$, where τ_r is the relaxation time associated with the displacement of a single vortex flux line from an "equilibrium" position, and η_ℓ and μ_ℓ are the vortex viscosity and vortex mass per unit length, respectively. The gap limited cutoff frequency is $\Omega_\Delta \approx \frac{2}{\hbar}\Delta$.

Various contributions to the vortex mass μ_ℓ are well known. These include the mass due to the kinetic energy of the core, μ_ℓ^{core}, and that arising from the static electromagnetic energy of the vortex, μ_ℓ^{em}, first calculated by Suhl.[24] Additional contributions to the dynamic vortex mass have been shown to arise from the inertia of quantum excitations of the quasiparticles within the vortex core having longitudinal and transverse components with respect to the vortex velocity, $\mu_\ell^{\|e,h}$ and $\mu_\ell^{\perp e,h}$,[25] and from a strain field arising from the torsional shear deformations of the crystal lattice induced by the moving vortex, μ_ℓ^{sf}.[26–28] The mass contribution which will dominate at high frequencies is the electromagnetic mass μ_ℓ^{em}.[18] Blatter and Ivlev found $\Omega_\mu \sim 10\Omega_\Delta$ using the assumption that the value of τ_r is determined by the scattering rate of the quasiparticles in the normal vortex core. However, we consider instead that there are two separate intrinsic relaxation times: that of the quasiparticles within the vortex core,[29,30] τ_r^{core}, and that of displacements of a single

vortex flux line, τ_r^v, with $\tau_r^v \gg \tau_r^{core}$ as the melting transition is approached,[31] leading to the condition $\Omega_\mu < \Omega_\Delta$.

We work here with the expression of the melting line arrived at by Blatter and Ivlev in Ref. 18, which includes a term involving compressional modes of the elastic vortex lattice that was omitted in their initial work[21] when calculating the mean squared displacement amplitude $\langle u^2 \rangle$. For the latter expression, they found

$$H_m = \frac{4H_{c2}(0)\theta^2}{(1+\sqrt{1+4S\theta/t})^2}, \tag{3}$$

where the reduced temperature θ is given by $\theta = c_L^2\sqrt{\frac{\beta_{th}}{G_i}}(T_c/T-1)$, $S = q + c_L^2\sqrt{\frac{\beta_{th}}{G_i}}$, and $q = \frac{2\sqrt{\beta_{th}}}{\pi^3}\frac{Q_u}{\sqrt{G_i}}\Omega\tau_r$ is a parameter measuring the relative contribution of quantum and thermal fluctuations. $\tilde{Q}_u = \frac{e^2}{\hbar}\frac{\rho_N}{d}$ is the dimensionless quantum of resistance, $G_i = [T_c/H_c^2(0)\epsilon\xi^3(0)]^2/2$ is the Ginzburg number, c_L is the Lindemann number, $\beta_{th} \approx 5.6$,[18] τ_r is the vortex relaxation time, assumed to be the same as the scattering relaxation time of the quasiparticles in the vortex core given by the Drude formula $\sigma_N = e^2 n \tau_r / m$ (σ_N is the normal state conductivity, n is the free-carrier density, and m the electron mass), d is the distance between the superconducting planes, and Ω is the cutoff Matsubara frequency for Eq. (2).

Rather than using approximate constant values for the factors that go into the quantum parameter q, we include their appropriate exact temperature and field dependences. Since it is not known *a priori* whether the appropriate cutoff frequency is Ω_μ or Ω_Δ for all type-II superconductors, we will work with both. The differing expressions found below provide a means of experimentally determining the relevant cutoff mechanism by comparing to independent scaling results, as will be explained in the next section.

Starting with the expression for the kinetic cutoff frequency, using the Bardeen-Stephen expression for the viscous drag coefficient,[32]

$$\eta_\ell \approx \frac{\Phi_0^2 \sigma_N}{2\pi\xi^2}, \tag{4}$$

using the electromagnetic contribution of the vortex mass,[24]

$$\mu_\ell^{em} = \frac{1}{4\mu_0}\frac{\xi^2 H_c^2}{c^2}\left(\frac{\lambda}{\lambda_d}\right)^2 \tag{5}$$

with $H_c = \frac{\Phi_0}{2\sqrt{2}\pi\lambda\xi}$, and including the temperature dependence of $\xi = \xi_0/(1-t)^{1/2}$, we then have

$$\Omega_\mu \approx \sqrt{\frac{\eta_\ell}{\mu_\ell^{em}\tau_r^v}} = \frac{4c\lambda_d}{\xi_0}\sqrt{\frac{\pi\mu_0\sigma_N}{\tau_r^v}}(1-t)^{1/2}, \tag{6}$$

where λ_d is a shielding length a few times that of $(k_F)^{-1}$.

If instead the frequency cutoff in Eq. (2) is determined by the gap energy, then we will have

$$\Omega_\Delta \approx \frac{2\Delta_0}{\hbar}(1-t)^{1/2}. \tag{7}$$

Blatter and Ivlev heuristically argue that the relaxation time τ_r of the vortices is determined by the normal state conductivity based on the condition that the vortex velocity has to be consistent with the quasiparticle motion inside the vortex core, thus $\tau_r = \frac{m}{ne^2}\sigma$.[18] However, from the ansatz that the dynamical behavior of the vortices is determined by the critical properties of the fluctuation conductivity,[22] where the zero field ac fluctuation conductivity in the critical region scales as[5,33]

$$\sigma_f(\omega) \sim \xi^{z+2-d}\mathcal{S}(\omega\xi^z)$$

as $T \to T_c$, where $\xi \sim |T_c - T|^{-\nu}$, and with $\tau_r^v \sim \sigma_f$ in the limit $\omega \to 0$, we arrive at an expression for the single vortex relaxation time (to be evaluated along the melting line at $T = T_g$),

$$\tau_r^v = \tau_0\left(\frac{T}{T_c}\right)^s\left(1-\frac{T}{T_c}\right)^{-s}, \tag{8}$$

where $s \equiv \nu(z+2-d)$, which is in agreement with that found experimentally [Eq. (1)].

The ansatz of the vortex-glass theory of FFH[5] is that the zero field critical point is actually a multicritical point so that the vortex-glass melting line is actually a line of critical points. The generalization of the zero field transition to the in-field transition leads to the scaling expression for the vanishing of the dc resistivity as $T \to T_g^+$,

$$\rho = \sigma^{-1} \sim \xi_{VG}^{z+2-d} \sim (T-T_g)^{\nu(z+2-d)}.$$

From the FFH theory and the above ansatz of the single vortex relaxation time, it can be seen that the critical exponent which characterizes the vanishing of the resistivity as the melting transition of the vortex ensemble is approached from temperatures and/or fields above the transition also characterizes the shape of the melting line in the H-T plane.

If correlated columnar disorder is relevant, then the critical dynamics of the vortex ensemble is described by the Bose-glass model, where the diverging length scale is the wandering length of a localized vortex line transverse to the field direction, $\ell(T) \sim (T_{BG}-T)^{\nu'}$, and the relaxation time of a fluctuation diverges as $\tau \sim \ell_\perp^{z'}$, where ν' and z' are additional critical exponents.[6] The vortex dynamics in the melting region described by this model leads to a power-law scaling of the dc resistivity, $\rho(T)$, with the same form as that found by the FFH vortex-glass model with the exponent $s \to s'$, where s' is defined in accordance with the updated Bose-glass scaling relations for the resistivity,[8]

$$\rho_\perp = \ell^{d+\zeta-3-z}\tilde{\rho}_\pm^\perp(H_\perp \ell^{d-2}),$$

$$\rho_\parallel = \ell^{d-\zeta-1-z}\tilde{\rho}_\pm^\parallel(H_\perp \ell^{d-2}),$$

where ζ is an anisotropy exponent, with $\zeta = 1$ for unscreened long-range interactions and $\zeta = 2$ for correlated disorder. In the case when H is parallel to the columnar defects, the relevant resistivity is $\rho_\perp$, so then $s' \equiv \nu'(z'+3-\zeta-d)$, with $\zeta = 2$.

Whether the correct form for the critical exponent is the vortex-glass exponent s or the Bose-glass exponent s' can readily be determined by the angular dependence of the scaling of the resistivity at the melting transition, where, if the vortex ensemble is a Bose glass,[34]

$$\rho_{\perp}(t,\theta) = |t|^{\nu'_{\perp}(z'-2)} f_{\pm}(\theta/|t|^{\nu'_{\perp}}),$$

$$\rho_{\parallel}(t,\theta) = |t|^{\nu'_{\perp} z'} g_{\pm}(\theta/|t|^{\nu'_{\perp}}),$$

and by the well known cusp in the phase boundary $T_{BG}(H_{\perp})$, where the perpendicular field $H^{c}_{\perp}(T)$ at the Bose glass to vortex liquid transition varies as[8,34]

$$H^{c}_{\perp} \sim \pm [T_{BG}(0) - T]^{\nu'}.$$

The Bose-glass phase will eventually give way to the vortex-glass phase as the field increases sufficiently past the matching field (the field at which the number of vortex lines is equal to the number of columnar defects), so that the majority of the vortex lines are far away from the correlated disorder and their dynamical properties are dominated by point defects. The change in vortex dynamics along the melting transition will be reflected in the shape of the melting line, $H_g(T)$, through a change of the value of the critical exponent and of the quantum parameter q. For simplicity, we use below the vortex-glass exponent s, but it should be understood that $s \rightarrow s'$ in the case of a Bose glass.

Combining Eq. (6) with Eq. (8), and with all expressions to be evaluated at the melting temperature $T=T_g \equiv T_m$, we obtain the full expression for the kinetic cutoff frequency,

$$\Omega_{\mu} = \frac{4c\lambda_d}{\xi_0}\sqrt{\frac{\pi\mu_0\sigma_N}{\tau_0}}\left(\frac{T}{T_c}\right)^{-s/2}\left(1-\frac{T}{T_c}\right)^{(1+s)/2}. \quad (9)$$

Next we use the expression for the dimensionless quantum of resistance given in Ref. 3,

$$\tilde{Q}_u = \frac{e^2}{\hbar}\frac{\rho_N}{\epsilon\xi}, \quad (10)$$

and the field dependent expression of the Ginzburg number,[10]

$$G_i(H_g) \approx (G_i)^{1/3}\left(\frac{H_g}{H_{c2}(0)}\right)^{2/3}. \quad (11)$$

Combining Eq. (7) or (9) with Eqs. (8), (10), and (11), we arrive at the final expression for the value of the quantum parameter, $q_{[\mu,\Delta]}$, at the melting line $H_g(T)$,

$$q_{[\mu,\Delta]} = \frac{2\sqrt{\beta_{th}}}{\pi^3}\frac{\tilde{Q}_0\Omega_0\tau_0}{\sqrt{G_i(H_g)}}t^{\tilde{s}}(1-t)^{1-\tilde{s}} \quad (12)$$

with

$$\Omega_0[\mu,\Delta] = \left[\Omega_{\mu 0} \equiv \frac{4c\lambda_d}{\xi_0}\sqrt{\frac{\pi\mu_0\sigma_N}{\tau_0}}, \Omega_{\Delta 0} \equiv \frac{2\Delta_0}{\hbar}\right],$$

$\tilde{Q}_0 \equiv \frac{e^2}{\hbar}\frac{\rho_N}{\epsilon\xi_0}$, $\tilde{s}[\mu,\Delta]=[s/2,s]$, and $t \equiv T/T_c = T_g/T_c$. Combining Eq. (5) with Eq. (17), we have

$$H_g(t) = \frac{4H_{c2}(0)\dfrac{\beta_{th}c_L^4}{G_i(H_g)}(t^{-1}-1)^2}{\left(1+\sqrt{1+4\left[\dfrac{2\tilde{Q}_0\Omega_0\tau_0}{\pi^3}t^{\tilde{s}}(1-t)^{1-\tilde{s}}+c_L^2\right]\dfrac{c_L^2\beta_{th}}{G_i(H_g)}t^{-1}(t^{-1}-1)}\right)^2}. \quad (13)$$

The above expressions for the cutoff frequency Ω, the quantum parameter q, and the melting line expression $H_g(t)$ given in Eqs. (12) and (13) differ from those given in our previous work, Eqs. (5)–(7) in Ref. 22. As pointed out above, these differences arise primarily from the use of the melting line expression arrived at by Blatter and Ivlev in their later work,[18] given here in Eq. (3). Additional differences are due to the generalization of the expressions to encompass the use of either the kinetic cutoff frequency Ω_{μ} or the gap energy limiting frequency Ω_{Δ}. However, as can be seen in Fig. 1, both expressions describe the data for all samples equally well with the only major difference being the values obtained for the quantum parameters q_0 and Q_0. This is discussed further below.

It should be noted that the expression used for the field dependent Ginzburg number in Eq. (11) is arrived at from a melting line that follows the power-law form $H_m \sim \frac{H_{c2}(0)}{\sqrt{G_i}}(1-t)^{3/2}$, and so is strictly valid only for $T \gtrsim 0.6T_c$. In general, for a portion of the melting line that can be approximated by $H_m \sim \frac{H_{c2}(0)}{\sqrt{G_i}}(1-t)^{\alpha}$,

$$G_i(H_g) \approx (G_i)^{1/2\alpha}\left[\frac{H_g}{H_{c2}(0)}\right]^{1/\alpha}. \quad (14)$$

When performing a fit of Eq. (13) to melting line data, a temperature dependent expression for the Ginzburg number $G_i(T_g)$ is needed. This is obtained from the field dependent Ginzburg number by evaluating Eq. (14) at each known field $H_g(T)$ and inverting as a function of temperature.

Also, it should be noted that at finite frequencies, dispersive effects lead to[18,35]

$$\eta(\omega) \approx \Phi_0\rho_s\frac{\omega_0\tau_r^{core}(1-i\omega\tau_r^{core})}{(1-i\omega\tau_r^{core})^2+(\omega_0\tau_r^{core})^2}, \quad (15)$$

with $\rho_s = 2e|\psi|^2$ the superfluid density. However, away from the superclean limit ($\omega_0\tau_r \ll 1$) or for high frequencies ($\omega\tau_r$

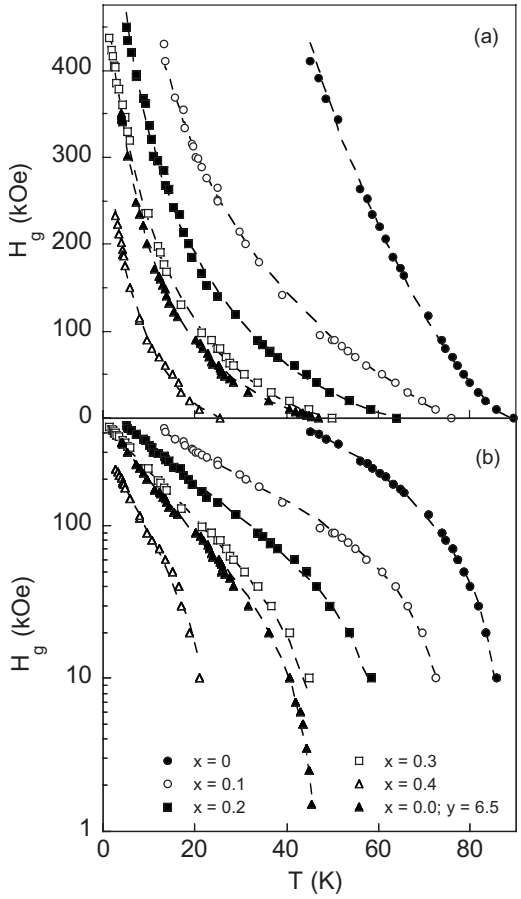

FIG. 1. (a) Fit of Eq. (13) to vortex-glass melting line, $H_g(T)$, data of $Y_{1-x}Pr_xBa_2Cu_3O_{6.97}(x=0-0.4)$ and $YBa_2Cu_3O_{6.5}$. (b) Same data as in (a) shown in a semilogarithmic plot to emphasize the quality of the fit to the low-field region.

$\gg 1$), dissipative dynamics[36] dominates and the Bardeen-Stephen result [Eq. (4)] is recovered.

An additional important result, addressed in more detail in the Appendix, is that the modified vortex-glass model of Rydh and co-workers[37,38] and the Coulomb-gas scaling model[39] are special cases of the model considered here.

IV. DISCUSSION

The melting line data $H_g(T)$ of the $Y_{1-x}Pr_xBa_2Cu_3O_{6.97}$ films and $YBa_2Cu_3O_{6.5}$ single crystal obtained in this study and that of a bulk MgB_2 sample and amorphous α-Mo_xSi_{1-x} film were fitted by Eq. (13). We discuss in detail below the results for the fits for the $Y_{1-x}Pr_xBa_2Cu_3O_{6.97}$ films and $YBa_2Cu_3O_{6.5}$ single crystals, shown in Fig. 1. The results for the MgB_2 and α-Mo_xSi_{1-x} samples are commented on in the next section.

Comparison of the values of c_L, s, and q_0 or Q_0 given in Table I to the values found in our previous work[22] shows overall good agreement. The values of c_L are in very good agreement for all samples, with differences ranging from 0% to ~12%. The values for s are in good agreement, with the exception of the $x=0$ optimally oxygenated sample. For all other samples, disagreement ranges from ~5% to 19%, which is not considered to be overly significant since the errors for the values of these exponents is estimated at ~10%–15%. For the $x=0$ sample, the values are 4.6 vs 3.33, an approximately 30% disagreement. The likely explanation for this larger discrepancy is that the data for this sample only extend to $T=0.5T_c$, whereas for the remaining samples the data extend over temperatures ranging from T_c down to $(0.03-0.17)T_c$. Thus there is more room for error in the fitting processes involved for either expression for the melting line. The values for the quantum parameter q_0, found using the melting equation given in this manuscript, are seen to be a factor of ~5–20 smaller than those for Q_0, found using the melting line expression in Ref. 22. As noted in our earlier work, the model leading to the initial melting line expression of Blatter and Ivlev, used in Ref. 22, did not include the thermal contribution of compressional modes. Since the quantum parameter is a measure of the strength of quantum to thermal fluctuations, the exclusion of the compressional modes will likely decrease the measure of thermal fluctuations, thus likely overestimating Q_0.

Using the values of $\epsilon=1/\gamma$, ρ_N, and q_0 in Table I, with $\lambda_d \approx k_F^{-1}$ [$k_F \sim 0.2$ Å^{-1} (Ref. 18)] and $G_i(0) \approx 10^{-2}$, we can then calculate values for Ω_0 and τ_0 using Eqs. (12) and (9). We find $\Omega_\mu \sim 10^3 \Omega_\Delta$ for $x=0.1-0.4$ and $y=6.5$, and Ω_μ

TABLE I. Values of the Lindemann number c_L, critical exponent $s \equiv \nu(z+2-d)$, and the quantum parameter $q_0 \equiv \tilde{Q}_0 \Omega_0 \tau_0$ using Eq. (13) for the data in Fig. 1. The error values are $\Delta c_L \sim 0.02$, for all c_L, and ≈15% for all values of s and q_0. The values of the anisotropy parameter γ for $Y_{1-x}Pr_xBa_2Cu_3O_{6.97}$ are from Ref. 40 and for $YBa_2Cu_3O_{6.5}$ are given in Ref. 41. The values of ξ are derived from the value of $H_{c2}(0)$ obtained from the fits to the data.

x	c_L	s	q_0	γ	ρ_N ($\mu\Omega$ m)	ξ (Å)
0	0.34	4.6	0.07	7.4	0.2	13
0.1	0.31	1.6	4.1	8.4	8.4	17
0.2	0.29	1.8	1.3	14.3	9.3	20
0.3	0.30	2.0	1.5	16.4	9.8	26
0.4	0.31	1.8	0.8	20.8	10.3	29
			$y=6.5$			
0	0.28	2.0	0.8	65	2.2	22

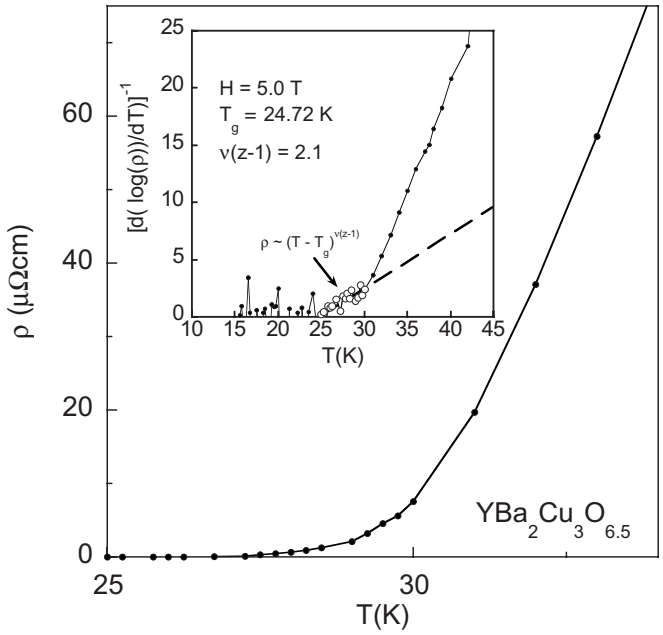

FIG. 2. Resistivity data, $\rho(T)$, and scaled resistivity data, $[d\log\rho(T)/dT]^{-1}$ vs T, of a $YBa_2Cu_3O_{6.5}$ single crystal.

$\sim 10^4\Omega_\Delta$ for $x=0$. This would imply that the correct expression for the quantum parameter is q_Δ, and thus, $\tilde{s}=s$. However, as shown by the example in Fig. 2 for $YBa_2Cu_3O_{6.5}$, the critical exponent $s\equiv\nu(z-1)$ obtained from scaling of the resistivity data $\rho(T)$ agrees well with the value of $\tilde{s}$ found from the fit to the melting line data by using Ω_μ [Eq. (9)] in Eq. (13) for all of the melting lines, i.e., $\tilde{s}=s/2$. This leads to an apparent contradiction, since the condition $\Omega=\min[\Omega_\mu,\Omega_\Delta]$ means we expect Ω to be given by Eq. (7).

This contradiction can be resolved if the effective vortex line mass is larger than the individual line mass μ_ℓ^{em} used in Eqs. (6) and (9). From Eq. (12), we can solve for τ_0 in terms of the experimentally determined fit parameters, giving

$$\tau_0=\left(\frac{q_0}{\tilde{Q}_0}\right)^2\frac{\pi^6}{4\beta_{th}}\frac{\mu_{em}}{\eta_\ell}. \tag{16}$$

Then, substituting Eq. (16) into Eq. (6) and assuming an effective mass $\mu^*=\alpha\mu_{em}$, we solve for the enhancement factor necessary to satisfy $\Omega_\mu=\Omega_\Delta$,

$$\alpha=\frac{\eta_\ell}{\mu_{em}}\frac{\tilde{Q}_0}{q_0}\frac{2\sqrt{\beta_{th}}}{\pi^3}\frac{1}{\Omega_\Delta}. \tag{17}$$

This gives $\alpha\sim 10^4$ for the $YBa_2Cu_3O_{7-\delta}$ film and $\alpha\sim 10^3$ for the remaining samples.

The friction encountered by a vortex line mass due to dissipation and quantum vortex tunneling has been considered by Blatter *et al.*[3] The dynamic vortex friction produces an enhanced and dispersive vortex effective mass, $\mu_\ell^*=\mu_\ell(1+\eta_\ell/|\omega|\mu_\ell)$, where ω is an inverse quantum tunneling time, η_ℓ is the total viscosity per unit length, and μ_ℓ is the total vortex mass per unit length. In the dissipative limit, the quantum tunneling time (in SI mks units) is found to be,[3]

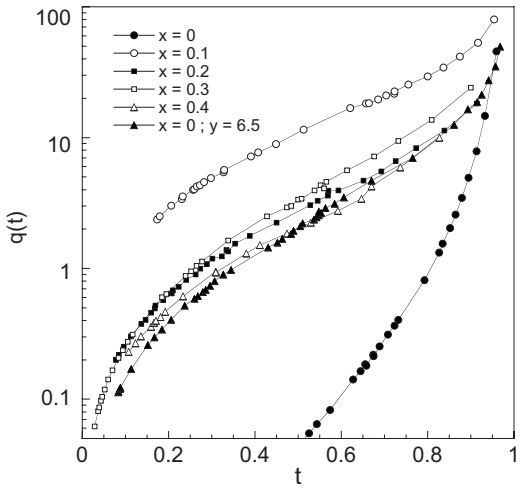

FIG. 3. The quantum parameter $q(t)$ measuring the relative contribution of quantum to thermal displacements of a single vortex line for the $Y_{1-x}Pr_xBa_2Cu_3O_{6.97}$ and $YBa_2Cu_3O_{6.5}$ samples obtained from the fit of the melting line data to Eq. (13).

$$t=\frac{\mu_0\eta_\ell L_c^2}{4\pi\epsilon_o},$$

where $\epsilon_o=[\Phi_0/4\pi\lambda]^2$ is the basic energy scale of the vortex line energy, $\epsilon_\ell=\epsilon_o\ln(\lambda/\xi)$, and L_c is the collective pinning length of a segment of the vortex along the vortex length. With $\omega=t^{-1}$, the effective electromagnetic vortex mass μ_{em}^* is given (in mks units) by

$$\mu_{em}^*\approx\mu_{em}\left(1+\frac{\mu_0\eta_\ell^2L_c^2}{4\pi\epsilon_o\mu_{em}}\right). \tag{18}$$

A lower limit of the value of the collective pinning length L_c can be set by the size of the vortex core diameter, giving $L_c\geq 2\xi_0$. This limit is reasonably chosen, since, for a displacement of a segment of the vortex core smaller than ξ, the vortex flux line distortion becomes large and leads to a breakdown of simple elastic vortex motion.[3] Using $\lambda\approx 1400-2900$ Å,[40] then $\epsilon_o\approx(0.3-1)\times 10^{-12}$ J/m. Using the values of ρ_N and ξ given in Table I, the values of $\eta_\ell(0)$ are in the range $\eta_\ell(0)\approx 10^{-6}-10^{-9}$ N s/m^2. Finally, the lower limit of the effective electromagnetic vortex mass is found to be $\mu_{em}^*\sim(10^3-10^6)\mu_{em}$, a considerable increase. Substituting the effective mass values back into Eq. (12), and solving again for Ω_0 and τ_0 for each sample, we find $\Omega_{\mu^*}\lesssim(10^{-1}-10^{-2})\Omega_\Delta$. It is seen then that dissipation from quantum tunneling produces an enhancement of the high frequency electromagnetic contribution to the vortex mass μ_{em}^* sufficient to result in a lowering of the cutoff frequency Ω_{μ^*} such that $\Omega_{\mu^*}<\Omega_\Delta$. Thus, the disagreement between the values found for the FFH critical exponent and the single vortex relaxation time exponent can be resolved.

The values of the quantum parameter as a function of temperature, $q(t)$, for each of the samples are shown in Fig. 3. The results here are in contrast to what might be expected, in that the value of $q(t)$ increases with temperature, becoming very large as $T\to T_c$. This can be understood physically

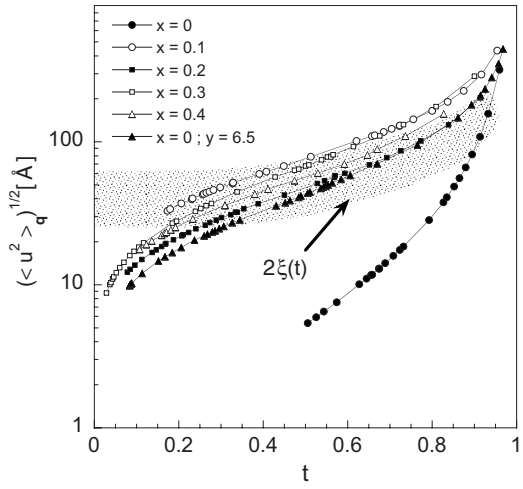

FIG. 4. Temperature dependence of the quantum tunneling length scale defined by the square root of the quantum contribution to the mean squared displacement field $\langle u^2\rangle_q$ for the $Y_{1-x}Pr_xBa_2Cu_3O_{6.97}$ and $YBa_2Cu_3O_{6.5}$ films. The shaded region corresponds to the range of the diameters of the vortex cores, $d \sim 2\xi$.

from the contribution of various intrinsic properties: First, the line tension $\epsilon_\ell \propto \lambda^{-2}$ vanishes as $(1-t)$. So, while the effect of quantum fluctuations is significant at low temperatures, the quantum tunneling of a segment of the vortex flux line, in this case a pancake vortex, becomes easier as the flux line becomes more flexible with increasing temperature. Additionally, we would expect quantum tunneling to be easier at lower fields (higher temperatures) with the increased distance between the flux lines. Also, with the dynamic behavior of the vortices along the melting line set by the relaxation time τ_r^v, which follows from the scaling properties of the fluctuation conductivity, the superfluid density plays a significant role in the problem of the melting transition. Experimental evidence, at least in the case of $YBa_2Cu_3O_{6.95}$, indicates that the field dependence penetration depth λ_{ab}, in magnetic fields up to 6 T, seems to indicate that $\lambda_{ab}(H=H_{c2}) \approx 2\lambda_{ab}(H=0)$ at $T=0$.[42,43] Additionally, Amin *et al.*,[44] studied the consequences of the nonlinear, nonlocal, and nonanalytic nature of the effect of the anisotropic superconducting gap on the effective penetration depth and found, that, contrary to common belief, the effective penetration depth is not a linear function of the magnetic field, a result that is in agreement with the experimental data of Ref. 42. From the temperature and field dependences of the penetration depth λ, it can be seen that the superfluid density in the region of the vortex solid melting line is larger at high fields than at low fields. This adds to the impedance of the tunneling process, since this means moving a core of normal electrons through a more dense superfluid. It is predicted that the melting line will terminate prior to reaching H_{c2} when it gives way to what is referred to as a quantum vortex liquid state (QVL).[3,18,21,45] Experimental evidence for the QVL state was found in α-Mo_xSi_{1-x} amorphous films at fields above $H \approx 0.9B_{c2}(0)$,[46,47] so it is quite possible that the melting line terminates well before any strong field suppression effects of the superfluid density are relevant. Lastly, as can be seen in Fig. 4, and discussed below, the distance over which quantum fluctuations displace the vortex is of the order of the size of the vortex core. At low fields, as the melting line approaches the critical temperature T_c, the size of the vortex cores at the melting transition increases as $(1-T/T_c)^{-1/2}$, thus the distance over which a quantum fluctuation displaces a vortex line segment grows accordingly.

An important aspect of the physical picture to be kept in mind is that disorder *promotes* quantum fluctuations, as can be seen by the expressions for $\tilde{Q} \propto \rho_N$ and $\Omega_\mu \propto \sqrt{\rho_N}$, so that $q_{[\mu,\Delta]} \propto [\sqrt{\rho_N}, \rho_N]$. This is understood by the fact that the vortices need somewhere to tunnel to, so then, up to a certain level of disorder, the value of q should increase as random disorder increases, and then decrease as the increasing disorder begins to shorten the distance over which a vortex segment tunnels. This effect can be seen in Fig. 3, where the clean $YBa_2Cu_3O_{7-\delta}$ film has a much lower value of $q(t)$ than the doped $Y_{1-x}Pr_xBa_2Cu_3O_{6.97}$ and oxygen deficient $YBa_2Cu_3O_{6.5}$ films, and also from the result where the $x=0.1$ sample has a notably larger value of $q(t)$ than the other samples. This same behavior can also be seen in Fig. 4, where the distance over which quantum fluctuations displace the vortex core is plotted, shown as the square root of the quantum contribution to the mean squared displacement field $\langle u^2\rangle_q$ versus the reduced temperature t, where[18]

$$\langle u^2\rangle_q \approx \frac{4}{\pi^2} Q\Omega\tau_r\xi^2.$$

The quantum tunneling length is shortest in the clean $YBa_2Cu_3O_{7-\delta}$ film, longest in the $x=0.1$ film, and close to or less than the $x=0.1$ tunneling length in the remaining films. The apparent nonmonotonic dependence of the quantum tunneling length on x for the $x=0.1-0.4$ films is likely attributable to the error of $\sim 15\%$ of the values shown. For comparison, the range of the size of the vortex cores, $d \sim 2\xi$, over all the samples is indicated by the range of the shaded region. With the exception of the $YBa_2Cu_3O_{7-\delta}$ sample, it is observed that, over most of the temperature range, the quantum fluctuations smear the core over a distance that is comparable to the size of the core, a result that is in agreement with the observation of Blatter and Ivlev for $YBa_2Cu_3O_{7-\delta}$, where they used a constant value of q and the zero temperature value of the coherence length ξ_0.[18,21]

The fraction of the quantum contribution to the displacement of the vortex line to the total displacement necessary for melting of the vortex lattice, $\sqrt{\langle u^2\rangle_q}/c_L a_\Delta$, where the critical displacement is defined by the Lindemann criterion, $\langle u^2\rangle \approx c_L^2 a_0^2$ $[a_\Delta = (2/\sqrt{3})^{1/2} a_0]$, is shown in Fig. 5. The contribution of quantum fluctuations to the melting of the vortex lattice is found to be a significant to dominant part of the melting process.

We recognize that the above result is both unexpected and contrary to the results of Blatter and Ivlev,[18] wherein they found that quantum fluctuations *will not be* relevant at temperatures near T_c. They reached this conclusion by examining the dynamical response of the supercurrent flow encircling a moving vortex. Specifically, the question to be addressed in determining whether or not quantum fluctua-

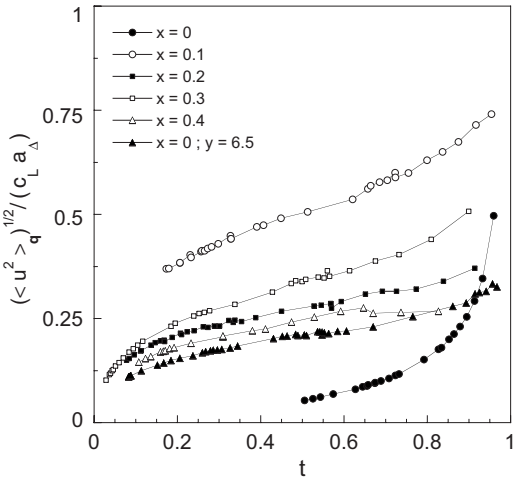

FIG. 5. Fraction of the quantum contribution to the mean squared displacement field to the total displacement, $\sqrt{\langle u^2\rangle_q/\langle u^2\rangle_{T_m}}$, at the melting transition, where $\langle u^2\rangle_{T_m} \approx c_L^2 a_0^2$ is the Lindemann criterion for the melting of the vortex lattice. The error of the values shown is estimated as ~10%.

tions are relevant to the melting process of the solid vortex ensemble is "will the quantum fluctuations of the vortex core be felt by neighboring vortices?" Blatter and Ivlev found that if the supercurrent surrounding the vortex core is able to follow the motion of the core, then neighboring vortices will be affected; if not, then the fluctuating vortex core will be screened at a short distance by the normal current flow driven by the scalar potential in the core region.

This question is first addressed by considering the ratio of the quasiparticle and London current densities,[18]

$$\frac{J_N}{J_L} = \frac{4\pi\lambda^2\sigma_N(\omega_n)|\omega_n|}{c^2} \sim \frac{|\omega_n|\tau_r}{1+|\omega_n|\tau_r}\frac{1}{\Delta^2(T)}, \tag{19}$$

where τ_r is the normal state (quasiparticle) scattering time and ω_n are the Matsubara frequencies (associated with the quantum fluctuations of the vortex core) which are limited by the cutoff frequency $\Omega=\min[\Omega_\mu,\Omega_\Delta]$.

From Eq. (19) above, it is seen that, at low temperatures, for both vanishing frequencies and for high frequencies the London currents are dominant. Based on the *assumption that* ω_n *remains finite* as $T\to T_c$ and also with $\Delta(T)\to 0$ as $T\to T_c$, Blatter and Ivlev then found, for temperatures near T_c, that $J_N \gg J_L$, and logically concluded that quantum fluctuations are not relevant to the melting process at temperatures near T_c.

However, if one accepts the empirically determined expression for the single vortex relaxation time, τ_r^v, and the resulting expression for the (mass limiting) cutoff frequency $\Omega_\mu \sim (1-t)/\sqrt{\tau_r^v}$, *which goes to zero* as $T\to T_c$, then the upper limit of the Matsubara frequencies ω_n must also vanish in the same manner as $T\to T_c$. Then, with $\omega_n \leqslant \Omega_\mu$, and with Ω_μ vanishing more rapidly than $1/\Delta^2(T)$ diverges as $T\to T_c$, the result is instead that $J_L \gg J_N$, from which it follows that quantum fluctuations of the vortex core, in fact, remain very relevant to the melting process for all $T<T_c$.

To examine the question of the relevancy of quantum fluctuations further, Blatter and Ivlev[18] also considered the related issue of dissipation due to vortex motion close to T_c. By assuming that their previous conclusion was incorrect and instead that vortex motion remains coupled to the London currents as $T\to T_c$, they arrived at an expression for the power dissipated by normal currents outside the vortex core as $T\to T_c$, wherein $P\sim\sigma_N\Phi_0^2u^2\omega_n^2/\ell^2c^2$. Here, u is the magnitude of the total vortex displacement, and $\ell_E\sim\xi(0)$ is the charge imbalance length associated with the normal current flow around the core. Again, *assuming that* ω_n *remains finite* as $T\to T_c$, then P remains finite as $T\to T_c$, from which it follows that their counter assumption that the vortex motion remains coupled to the London currents is incorrect.

However, if the empirically arrived at expression for $\Omega_\mu=\Omega_0 t^{-s/2}(1-t)^{(1+s)/2}$ is used, then the dissipation based argument is also overcome, since ω_n is limited by Ω_μ which goes to zero as $T\to T_c$. The vanishing behavior of P as $T\to T_c$ can be found by using the following relations:

$$\langle u^2\rangle|_{T=T_m} = c_L^2 a_0^2, \tag{20}$$

$$a_0^2 = \frac{\Phi_0}{H}, \tag{21}$$

$$H_m|_{T\gtrsim 0.4T_c} \approx H_0[(1-t)/t]^{s/2}. \tag{22}$$

Then as $T\to T_c$,

$$P \sim \frac{\sigma_N\Phi_0}{\ell_E^2c^2}u^2\Omega^2 \sim (1-t)^{1/2}. \tag{23}$$

The results above, based on the empirically observed single vortex relaxation time τ_r^v, are *independent* of the ansatz that the scaling properties of the fluctuation conductivity are responsible for the single vortex relaxation time. However, within the context of this ansatz, these results are readily understood by considering the following: With the fluctuation conductivity responsible for the time scale over which vortex motion takes place, then, as the critical point $(H=0,T=T_c)$ is approached, a critical slowing down of the fluctuation induced motion of the vortex core would be expected. Naively, we would anticipate this time scale to diverge as $\tau\sim(1-T/T_c)^{-\zeta}$, for some positive exponent ζ, and that the frequency of the quantum fluctuations would go to zero as $\omega_n\sim 1/\tau$. Then, so long as $\zeta\geqslant 1$, Eq. (19) above remains finite as $T\to T_c$, implying the continued relevance of quantum fluctuations. A more restrictive value for ζ requires $P\sim u^2\Omega^2\to 0$ as $T\to T_c$, so then we must have $\zeta>s/2$.

V. VORTEX-GLASS MELTING LINES OF MgB_2 AND α-Mo_xSi_{1-x}

To further demonstrate that the melting line equation developed here is not limited to just high-T_c compounds, we have fitted Eq. (13) to vortex-glass melting line data of two very different compounds, MgB_2 and α-Mo_xSi_{1-x}.

The vortex-glass melting line, $H_g(T)$, of a bulk sample of MgB_2 was determined by a scaling of the dc resistive tran-

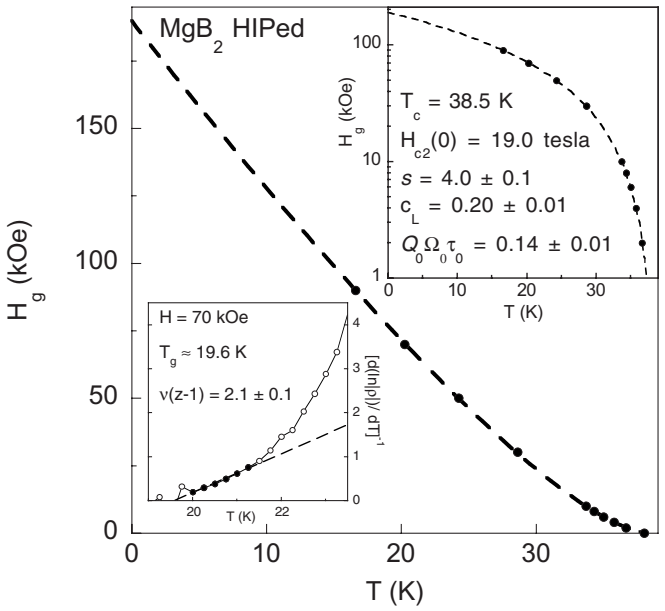

FIG. 6. Fit of Eq. (13) to vortex glass melting line, $H_g(T)$, data of a bulk MgB_2 sample prepared by hot isostatic pressing (HIP). The upper inset shows the same data on a semilogarithmic plot. The lower inset shows resistivity data plotted as $[d \ln \rho(T)/dT]^{-1}$ vs T, demonstrating vortex-glass behavior, with $\rho(T) \sim (T-T_g)^{\nu(z-1)}$. The value of the critical exponent $s \approx 4.0$, obtained from the fit of Eq. (13) to the melting line data, is a factor of 2 greater than that found from scaling of the resistivity data, $\nu(z-1) \approx 2.1$. Data taken from Ref. 48.

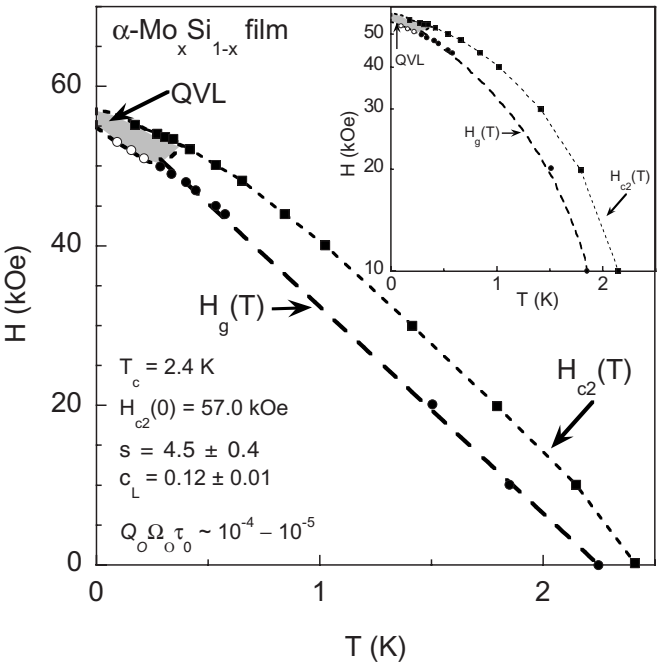

FIG. 7. Fit of Eq. (13) to vortex-glass melting line, $H_g(T)$, data of a 100 nm thick film of α-Mo_xSi_{1-x} ($x \approx 0.44$). The inset shows the same data on a semilogarithmic plot. Data taken from Ref. 46. Okuma *et al.* found $\nu \sim 1$ and $z \sim 5.4$ for all fields $H \lesssim 5$ T from scaling of the dc resistivity by the form $\rho(T) \sim (T/T_g - 1)^{\nu(z-1)}$. At fields above 5 T, Okuma *et al.* found evidence from scaling analysis of the ac resistivity ρ_{ac} of a quantum liquid vortex state. Thus the melting line terminates prior to connecting to the upper critical field line $H_{c2}(T)$.

sition in accordance with the vortex-glass theory of FFH, $\rho(T) \sim (T-T_g)^{\nu(z-1)}$.[48] The fit of Eq. (13) to the data is shown in Fig. 6. The SVRT exponent value of $s=4.0$, obtained from the fit to the melting line data, was found by assuming that the limiting frequency $\Omega=\Omega_\mu$, i.e., $\tilde{s}=s/2$, as in the case for the high-T_c samples considered above. However, the exponent $s_{VG} \equiv \nu(z-1) \approx 2.1$, found from the scaling of the resistivity data, is approximately equal to half of the exponent s found from the fit of the melting line equation. If instead we use $\Omega=\Omega_\Delta$, i.e., $\tilde{s}=s$, we obtain the SVRT exponent value of $s=2.0$, in agreement with the value of s_{VG}. This indicates that the energy gap Δ provides the scale of the energy cutoff which limits the dynamical properties of the vortices, and therefore, the correct expression for the quantum parameter q in this case is q_Δ [Eq. (12)].

The vortex-glass transition has been shown directly to exist in amorphous films of the low temperature superconductor a-Mo_xSi_{1-x} down to $T \sim 0.04T_c$ by measurements of the dc and ac complex resistivities in constant fields.[46,47] The transition was identified by the scaling relation of the dc resistivity stated above and from the ac resistivity which, in agreement with FFH theory, follows a power-law frequency dependence $\rho_{ac} \propto f^{(z-1)/z}$; the phase has a frequency-independent value $\phi_g=(\pi/2)(z-1)/z$. The fit of Eq. (13) to the a-Mo_xSi_{1-x} data is shown in Fig. 7. In this case, the exponent obtained from the melting line fit, $s \approx 4.5$, agrees well with the exponent $\nu(z-1) \approx 4.4$ found by vortex-glass scaling of the resistivity.

VI. SUMMARY

The vortex-glass melting lines, $H_g(T)$, of epitaxial thin film $Y_{1-x}Pr_xBa_2Cu_3O_{6.97}$ samples ($x=0-0.4$) grown on $LaAlO_3$ substrates by pulsed laser ablation, as well as an ultrahigh purity oxygen deficient $YBa_2Cu_3O_{6.5}$ single crystal grown in a $BaZrO_3$ crucible, were measured in magnetic fields up to 45 T. Analysis of the evolution of vortex dynamic properties along the melting lines of each system was carried out in the context of a modified melting line expression based on the quantum-thermal-fluctuation model of Blatter and Ivlev.[18] We have also provided further evidence that the equation provides truly a universal description of the melting line in type-II superconductors by fitting to vortex-glass melting line data from the noncuprate non-high-T_c systems, MgB_2 and α-Mo_xSi_{1-x}.

The melting line equation developed here provides an experimental means for determining the physical mechanism responsible for the energy scale that limits vortex motion at high frequencies. By determining the exponent s from vortex- (or Bose-) glass scaling analysis of the resistive transitions and comparing the value of s to the value of the exponent $\tilde{s}$, obtained from the fit to the melting line data of Eq. (13), the appropriate cutoff frequency Ω_μ or Ω_Δ can be determined.

It is found that the effective vortex mass is enhanced significantly by quantum fluctuations in the $Y_{1-x}Pr_xBa_2Cu_3O_{6.97}$

and $YBa_2Cu_3O_{6.5}$ samples studied here, leading to a value of the kinetic cutoff frequency $\Omega_\mu \ll \Omega_\Delta$. By examining the values of the quantum parameter as a function of temperature, $q(t)$, it is shown that quantum fluctuations play an important role in the physics of the vortex solid to vortex liquid transition. The value of $q(t)$ is found to increase significantly with temperature, becoming very large as $T \to T_c$. This is explained primarily due to the increase of the size of the vortex cores as the melting line approaches the critical temperature T_c, the distance over which quantum fluctuations displace a segment of the vortex flux line. The vanishing line tension $\epsilon_\ell \propto \lambda^{-2} \sim (1-t)$ and reduced superfluid density high-temperature/low-field region also likely contribute to quantum tunneling effects. The quantum tunneling length is found to be shortest in the relatively clean $YBa_2Cu_3O_{7-\delta}$ film, particularly at low temperatures. The tunneling distance is longest in the $x=0.1$ film, and similar to or less than that of the $x=0.1$ sample for the remaining films. This is understood by the physical scenario wherein disorder actually promotes quantum fluctuations, up to a point.

ACKNOWLEDGMENTS

This research was sponsored by the U.S. Department of Energy (DOE) under Research Grant No. DE-FG02-04ER46105. A portion of this work was performed at the National High Magnetic Field Laboratory, which is supported by NSF Cooperative Agreement No. DMR-0084173, by the State of Florida, and by the DOE.

APPENDIX A: MODIFIED VORTEX GLASS MODEL

Recently, Rydh, Rapp, and Andersson[37,38] (RRA) developed a modified vortex-glass (MVG) model based on the original model of Fisher *et al.*[5] and the empirically observed equation for the vortex-glass melting line by Lundqvist *et al.*,[49] where

$$B_m \approx \frac{1.85\Phi_0}{(\gamma d)^2}\left[\frac{(1-t)}{t}\right]^\alpha, \tag{A1}$$

with d the interlayer spacing and $\alpha \approx 1$. RRA arrived at a scaling law for the vanishing of the resistivity as the critical temperature T_g is approached, such that resistivity data taken in various constant magnetic fields will collapse onto a single curve when it is plotted as

$$\left[\frac{\rho(T)}{\rho_N}\right] \quad \text{vs} \quad \frac{T(T_c-T_g)}{T_g(T_c-T)} - 1. \tag{A2}$$

Additionally, Lundqvist *et al.* used the expression of the vortex lattice melting line arrived at by Blatter and Ivlev to lend support to the melting line equation. It is easily seen that Eq. (A1) can be recovered as a high q limiting case of Eq. (13) where $\alpha = \tilde{s}$.

APPENDIX B: COULOMB-GAS MODEL

The scaling laws from the Coulomb-gas (CG) scaling model[39] are nearly equivalent to those found from the modified vortex-glass thermal depinning model of Rydh and co-workers.[37,38] This can be seen simply by examining the scaling functions of the resistivity in the two cases. In the CG model, the resistivity data $\rho(T)$ is predicted to scale such that for all applied magnetic fields in the relevant regime, the data will collapse onto a single curve when plotted as

$$\ln\left[\frac{\rho(T)}{\rho_N}\right] \quad \text{vs} \quad \frac{T(T_c-T_g)}{T_g(T_c-T)}. \tag{B1}$$

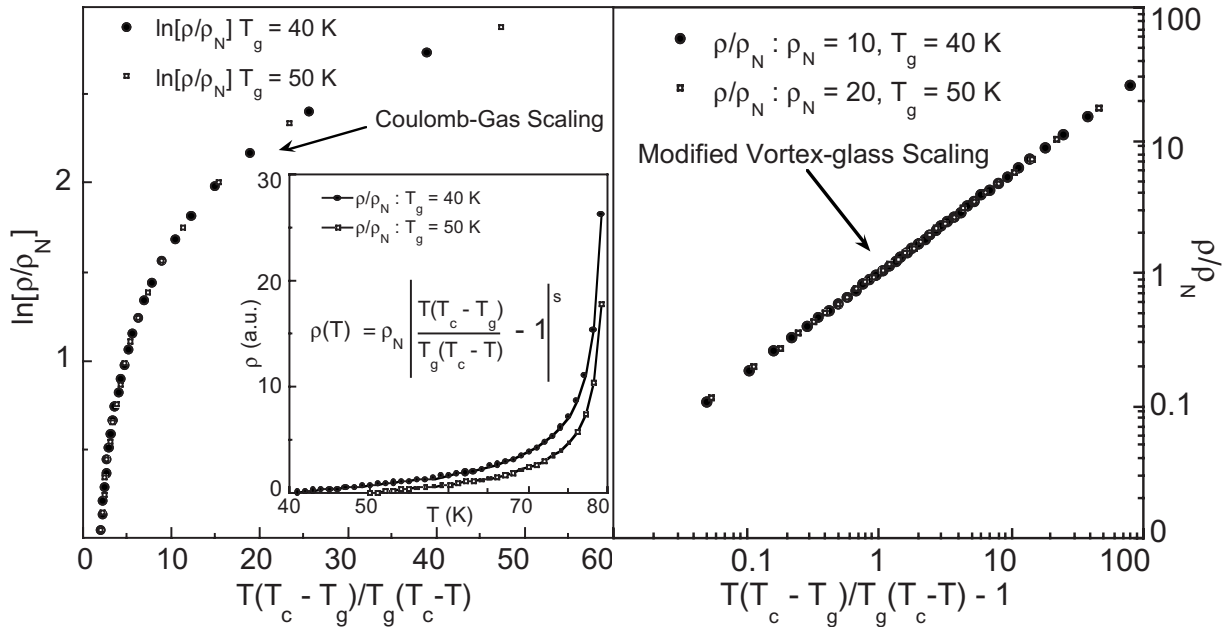

FIG. 8. Resistivity data generated from the modified vortex-glass relation $\rho(T,B) = \rho_N \left|\frac{T(T_c-T_g)}{T_g(T_c-T)} - 1\right|^s$, plotted according to the Coulomb-gas (left panel) and modified vortex-glass (right panel) scaling laws. Notice the linear (on a log-log plot) behavior of the data in the modified vortex-glass plot, a key indicator of vortex-glass behavior.

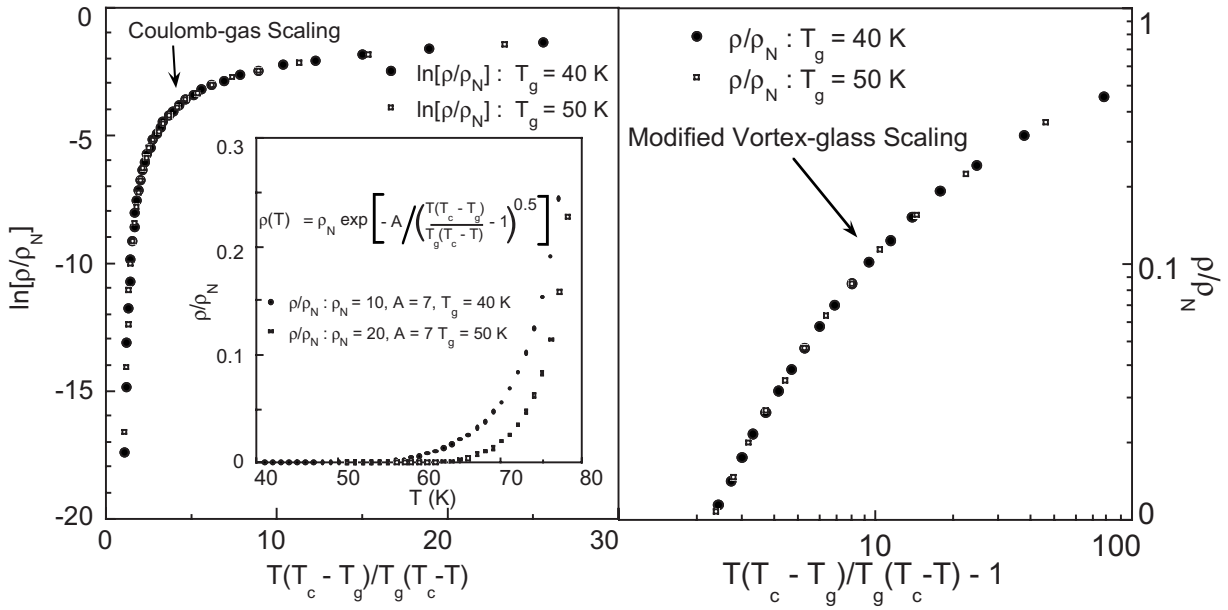

FIG. 9. Resistivity data generated from the Coulomb-gas relation $\ln\left[\frac{\rho(T,B)}{\rho_N}\right]=-A/\left[\frac{T(T_c-T_g)}{T_g(T_c-T)}-1\right]^{0.5}$, plotted according to the CG (left panel) and MVG (right panel) scaling laws. Note the lack of linear (on a log-log plot) behavior of the data in the MVG plot, indicating that vortex-glass behavior does occur in this case.

RRA noted that their scaling law is very similar to the CG scaling relation, and surmised that there is a likely connection between the generalized Coulomb-gas model and their modified vortex-glass model. The situation is thus as follows: If resistivity data will scale according to the CG model, it will also scale according to the MVG model, and vice versa.

This equivalence is shown in Fig. 8, where resistivity data for two different magnetic fields that were generated from the MVG relation

$$\rho(T,B)=\rho_N\left|\frac{T(T_c-T_g)}{T_g(T_c-T)}-1\right|^s \tag{B2}$$

are plotted according to both scaling relations.

However, it is possible to distinguish between the two cases. If, as is shown in Fig. 9, we plot resistivity data which were generated from the CG relation instead,

$$\ln\left[\frac{\rho(T,B)}{\rho_N}\right]=-A\Big/\left[\frac{T(T_c-T_g)}{T_g(T_c-T)}-1\right]^{0.5}, \tag{B3}$$

the data can again be seen to collapse in either case; *however*, the data fail to exhibit the predicted power-law behavior in the MVG scaling plot. Thus, it is quite obvious, from a formalistic and phenomenological examination, that the CG model is a special case or subset of the MVG model, which is itself a special case (the large q limit) of Eq. (13).

We reemphasize that, for a system which behaves in accordance with the modified vortex-glass model, electrical resistivity data in the region of vanishing resistivity will scale in agreement with both the MVG and CG scaling laws. The conformity of the resistance data to the scaling expressions of both models is not the case, however, for resistivity data from a system that behaves according to the Coulomb-gas model. It should then be recognized that, for a system whose vortex solid to vortex liquid transition phase boundary, $H_g(T)$, is described by Eq. (13), resistivity data in the region of the transition will conform to the Coulomb-gas scaling relation in addition to the vortex-glass or modified vortex-glass scaling laws. This, however, does not imply that the physics of the system is governed by the Coulomb-gas model.

[1] A. Schilling, R. A. Fisher, N. E. Phillips, U. Welp, D. Dasgupta, W. K. Kwok, and G. W. Crabtree, Nature (London) **382**, 791 (1996).
[2] M. J. W. Dodgson, V. B. Geshkenbein, H. Nordborg, and G. Blatter, Phys. Rev. Lett. **80**, 837 (1998).
[3] G. Blatter, M. V. Feigel'man, V. B. Geshkenbein, A. I. Larkin, and V. M. Vinokur, Rev. Mod. Phys. **66**, 1125 (1994).
[4] M. P. A. Fisher, Phys. Rev. Lett. **62**, 1415 (1989).
[5] D. S. Fisher, M. P. A. Fisher, and D. A. Huse, Phys. Rev. B **43**, 130 (1991).
[6] D. R. Nelson and V. M. Vinokur, Phys. Rev. Lett. **68**, 2398 (1992); Phys. Rev. B **48**, 13060 (1993).
[7] T. Giamarchi and P. Le Doussal, Phys. Rev. B **52**, 1242 (1995); **55**, 6577 (1997).
[8] J. Lidmar and M. Wallin, Europhys. Lett. **47**, 494 (1999).
[9] T. Hwa, D. R. Nelson, and V. M. Vinokur, Phys. Rev. B **48**, 1167

(1993).
[10] *Conventional and High-T_c Superconductors*, edited by K. H. Bennemann and J. B. Ketterson, The Physics of Superconductors Vol. I (Springer-Verlag, Berlin, 2003), pp. 789–800.
[11] M. B. Gaifullin, Y. Matsuda, N. Chikumoto, J. Shimoyama, and K. Kishio, Phys. Rev. Lett. **84**, 2945 (2000).
[12] G. I. Menon, Phys. Rev. B **65**, 104527 (2002).
[13] M. J. W. Dodgson, V. B. Geshkenbein, and G. Blatter, Physica B **280**, 220 (2000); M. J. W. Dodgson, A. E. Koshelev, V. B. Geshkenbein, and G. Blatter, Phys. Rev. Lett. **84**, 2698 (2000).
[14] D. R. Nelson and B. I. Halperin, Phys. Rev. B **19**, 2457 (1979).
[15] J. Kierfeld and V. Vinokur, Phys. Rev. B **61**, R14928 (2000).
[16] E. H. Brandt, Phys. Rev. Lett. **63**, 1106 (1989).
[17] A. Houghton, R. A. Pelcovits, and A. Sudbø, Phys. Rev. B **40**, 6763 (1989).
[18] G. Blatter and B. I. Ivlev, Phys. Rev. B **50**, 10272 (1994).
[19] G. P. Mikitik and E. H. Brandt, Phys. Rev. B **64**, 184514 (2001); **68**, 054509 (2003).
[20] J. Kierfeld and V. Vinokur, Phys. Rev. B **69**, 024501 (2004).
[21] G. Blatter and B. Ivlev, Phys. Rev. Lett. **70**, 2621 (1993).
[22] B. J. Taylor and M. B. Maple, preceding paper, Phys. Rev. B **76**, 014517 (2007).
[23] M. Charalambous, R. H. Koch, T. Masselink, T. Doany, C. Feild, and F. Holtzberg, Phys. Rev. Lett. **75**, 2578 (1995).
[24] H. Suhl, Phys. Rev. Lett. **14**, 226 (1965).
[25] N. B. Kopnin and V. M. Vinokur, Phys. Rev. Lett. **81**, 3952 (1998).
[26] E. M. Chudnovsky and A. B. Kuklov, Phys. Rev. Lett. **91**, 067004 (2003).
[27] Ji-Min Duan and Eugen Šimánek, Phys. Lett. A **190**, 118 (1994).
[28] M. W. Coffey, Phys. Rev. B **49**, 9774 (1994).
[29] C. Caroli, P. G. de Gennes, and J. Matricon, Phys. Lett. **9**, 307 (1964).
[30] K. Karrai, E. J. Choi, F. Dunmore, S. Liu, H. D. Drew, Qi Li, D. B. Fenner, Y. D. Zhu, and Fu-Chun Zhang, Phys. Rev. Lett. **69**, 152 (1992).
[31] L. T. Sagdahl, S. Gjølmesli, T. Laegreid, K. Fossheim, and W. Assmus, Phys. Rev. B **42**, R6797 (1990).
[32] J. Bardeen and M. J. Stephen, Phys. Rev. **140**, A1197 (1965).
[33] M. E. Fisher, M. N. Barber, and D. Jasnow, Phys. Rev. A **8**, 1111 (1973).
[34] D. R. Nelson and V. M. Vinokur, Phys. Rev. B **61**, 5917 (2000).
[35] N. B. Kopnin and M. M. Salomaa, Phys. Rev. B **44**, 9667 (1991).
[36] Z. Schlesinger, R. T. Collins, F. Holtzberg, C. Feild, S. H. Blanton, U. Welp, G. W. Crabtree, Y. Fang, and J. Z. Liu, Phys. Rev. Lett. **65**, 801 (1990).
[37] A. Rydh, Ö. Rapp, and M. Andersson, Phys. Rev. Lett. **83**, 1850 (1999).
[38] M. Andersson, A. Rydh, and Ö. Rapp, Phys. Rev. B **63**, 184511 (2001).
[39] P. Minnhagen, Rev. Mod. Phys. **59**, 1001 (1987).
[40] C. C. Almasan and M. B. Maple, Phys. Rev. B **53**, 2882 (1996).
[41] T. R. Chien, W. R. Datars, B. W. Veal, A. P. Paulikas, P. Kostic, Chun Gu, and Y. Jiang, Physica C **229**, 273 (1994).
[42] J. E. Sonier *et al.*, Phys. Rev. B **55**, 11789 (1997).
[43] J. E. Sonier *et al.*, Phys. Rev. Lett. **83**, 4156 (1999).
[44] M. H. S. Amin, I. Affleck, and M. Franz, Phys. Rev. B **58**, 5848 (1998).
[45] M. P. A. Fisher, G. Grinstein, and S. M. Girvin, Phys. Rev. Lett. **64**, 587 (1990).
[46] S. Okuma, Y. Imamoto, and M. Morita, Phys. Rev. Lett. **86**, 3136 (2001).
[47] S. Okuma, S. Togo, and M. Morita, Phys. Rev. Lett. **91**, 067001 (2003).
[48] S. Li, B. J. Taylor, N. A. Frederick, M. B. Maple, V. F. Nesterenko, and S. S. Indrakanti, Physica C **382**, 177 (2002).
[49] B. Lundqvist, A. Rydh, Yu. Eltsev, Ö. Rapp, and M. Andersson, Phys. Rev. B **57**, R14064 (1998).